

**DEVELOPMENT OF FÖRSTER RESONANCE  
ENERGY TRANSFER BASED HOMOGENEOUS  
IMMUNOASSAYS FOR DETERMINATION OF  
(R)-METHADONE**

**OOI MAY YUI**

**UNIVERSITI SAINS MALAYSIA**

**2016**

**DEVELOPMENT OF FÖRSTER RESONANCE  
ENERGY TRANSFER BASED HOMOGENEOUS  
IMMUNOASSAYS FOR DETERMINATION OF  
(R)-METHADONE**

by

**OOI MAY YUI**

**Thesis submitted in fulfillment of the requirements  
for the Degree of  
Doctor of Philosophy**

**August 2016**

## **ACKNOWLEDGEMENT**

This research was carried out in the Institute for Research in Molecular Medicine, University Science of Malaysia during the years 2011 – 2016. The financial support for the research from the Higher Institution Centre of Excellence (HICoE) and Research University grant from University Science of Malaysia are gratefully acknowledged.

I wish to express my sincere gratitude and appreciation to my supervisor, Prof. Dr. Tan Soo Choon, co-supervisor, Prof. Dr. Rusli Ismail and Dr Leow Chiuan Heng, for their guidance and support. Their kindness and generosity in sharing knowledge and experiences are very much appreciated.

I am very grateful to all staffs and students in the Institute for Research in Molecular Medicine and Usains Biomics Sdn. Bhd. for their kind assistance, guidance and providing the facilities throughout my research period.

Last but not least, I wish to express my warmest thanks my family and friends for their never ending support and encouragement. It has been a memorable journey working with my fellow lab mates in synthesis lab. They are very generous to share their experiences and knowledge when I was in time of need.

## TABLE OF CONTENTS

<b>ACKNOWLEDGEMENT</b>	ii
<b>TABLE OF CONTENTS</b>	iii
<b>LIST OF TABLES</b>	xvi
<b>LIST OF FIGURES</b>	xviii
<b>LIST OF ABBREVIATIONS</b>	xxv
<b>ABSTRAK</b>	xxx
<b>ABSTRACT</b>	xxxii
<b>CHAPTER 1 – GENERAL INTRODUCTION</b>	1
1.1 Drug testing	1
1.2 Immunoassay	2
1.2.1 Immunoassay system in drug testing	4
1.2.1(a) Radioimmunoassay (RIA)	4
1.2.1(b) Enzyme immunoassay (EIA)	5
1.2.1(c) Fluoroimmunoassay (FIA) & Fluorescence polarization immunoassay	6
1.2.1(d) Lateral flow immunoassay (LFIA)	7
1.2.2 Heterogeneous vs homogeneous immunoassay	8
1.3 Förster Resonance Energy Transfer (FRET)	9
1.3.1 FRET efficiency	10
1.3.2 Factors that affect FRET efficiency	11
1.3.2(a) Distance between donor-acceptor molecules	11
1.3.2(b) Spectral overlap of donor and acceptor	12

1.3.2(c)	Transition dipole orientations of the donor and acceptor	13
1.3.3	Fluorescent materials for used in FRET system	14
1.3.3(a)	Organic dyes	14
1.3.3(b)	Inorganic materials	17
1.3.3(b)(i)	Quantum dots	17
1.3.3(b)(ii)	Lanthanides	20
1.3.3(c)	Fluorophore of biological origin	23
1.4	Application of FRET technique	25
1.4.1	FRET based immunoassay	26
1.5	Problem Statement	27
1.6	Significance/Importance of Research	27
1.7	Aims of study	28
<b>CHAPTER 2 – METHADONE AND ITS ANTIBODIES</b>		<b>29</b>
2.1	Introduction	29
2.1.1	A brief history of methadone	30
2.1.2	Chemistry of methadone	31
2.1.3	Synthesis of methadone	32
2.1.4	Pharmacology of methadone	32
2.1.5	Pharmacokinetic of methadone	33
2.1.5(a)	Absorption	34
2.1.5(b)	Distribution	34
2.1.5(c)	Metabolism	36
2.1.5(d)	Excretion	36

2.1.6	Methadone in opioid dependence treatment	38
2.2	Aims and objectives	39
2.3	Reagents, chemicals and instrumentation	39
2.4	Methods	41
2.4.1	Modification of ( <i>R</i> )-methadone to ( <i>R</i> )-methadol hemisuccinate	41
2.4.1(a)	Reduction of carbonyl groups to form ( <i>R</i> )-methadol	41
2.4.1(b)	Addition of carboxylic groups	41
2.4.2	Characterization of ( <i>R</i> )-methadone and ( <i>R</i> )-methadol hemisuccinate	42
2.4.2(a)	Mass spectrometer analysis	42
2.4.2(b)	Nuclear magnetic resonance analysis (NMR)	43
2.4.3	Conjugation of ( <i>R</i> )-methadol hemisuccinate to horseradish peroxidase (HRP)	43
2.4.4	Purification of antibodies (Mab)	45
2.4.5	Development of an enzyme immunoassay	46
2.4.5(a)	Antibody coating protocol	46
2.4.5(b)	Optimization of enzyme immunoassay	47
2.4.5(c)	Determination of IC <sub>50</sub>	48
2.4.6	Validation of enzyme immunoassay	49
2.4.6(a)	Intra-assay	49
2.4.6(b)	Inter-assay	49
2.4.7	Antibodies cross-reactivity	49
2.5	Results and discussion	51
2.5.1	Characterization of ( <i>R</i> )-methadone and its derivatives	51
2.5.1(a)	Tandem mass spectroscopy analysis	51

2.5.1(b)	Nuclear magnetic resonance (NMR)	53
2.5.2	Purification of antibodies	55
2.5.3	Imprecision study of ELISA	55
2.5.4	Determination of antibodies IC <sub>50</sub>	57
2.5.5	Antibodies cross-reactivity studies	58
2.6	Conclusion	61
 <b>CHAPTER 3 – ORGANIC DYE AS FRET PAIR FOR IMMUNOASSAY DEVELOPMENT</b>		 63
3.1	Introduction	63
3.1.1	Fluorescein-5- isothiocyanate (FITC)	63
3.1.2	Rhodamine dyes	64
3.2	Aims and objectives	65
3.3	Reagents, chemicals and instrumentations	66
3.4	Methods	67
3.4.1	Selection of fluorescence dyes pair	67
3.4.2	Preparation of donor molecules	69
3.4.2(a)	Conjugation of FITC to anti ( <i>R</i> )-methadone monoclonal antibody(Mab)	69
3.4.2(b)	Characterisation of donor molecules	69
	3.4.2(b)(i) UV-VIS characterisation	69
	3.4.2(b)(ii) MALDI-TOF/TOF characterisation	70
3.4.3	Preparation of acceptor molecules	71
3.4.3(a)	Purification of ( <i>R,S</i> )-methadone from methadone syrup.	71

3.4.3(b)	Conjugation of ( <i>R,S</i> )-methadol hemisuccinate with lissamine rhodamine B diethylamine	72
3.4.3(c)	Characterisation of acceptor molecule	72
3.4.4	FRET experiments	72
3.4.5	FRET immunoassay platform development	73
3.4.5(a)	Optimization of donor: acceptor ratio	74
3.4.5(b)	Determination of optimum pH for immunoassay system	74
3.4.5(c)	Determination of optimum incubation time for immunoassay	74
3.4.5(d)	Determination of IC <sub>50</sub> of FRET immunoassay	75
3.4.5(e)	Verification of assay performance in human serum	75
3.4.6	Reproducibility studies of FRET immunoassay	75
3.4.6(a)	Intraday assay	75
3.4.6(b)	Interday assay	76
3.4.7	Linearity and functional sensitivity of FRET assay	77
3.4.8	Development of Point of Care (POC) FRET based immunoassay	77
3.5	Results and discussion	78
3.5.1	FRET dye pair selection	78
3.5.2	Characterisation of donor molecules	79
3.5.2(a)	UV-Vis characterisation	79
3.5.2(b)	MALDI-TOF/TOF characterisation	79
3.5.3	Characterisation of acceptor molecules	81
3.5.3(a)	Thin layer chromatography of RHB-EDA/Mtd	84
3.5.3(b)	Tandem mass spectroscopy analysis	85



	3.5.3(b)(i)	( <i>R,S</i> )-methadone that extracted from syrup	85
	3.5.3(b)(ii)	LRB-EDA/Mtd (acceptor molecule)	85
3.5.4	FRET experiments		86
3.5.5	FRET immunoassay platform optimization		88
	3.5.5(a)	Optimization of donor: acceptor ratio	88
	3.5.5(b)	pH	88
	3.5.5(c)	Incubation Time	90
	3.5.5(d)	IC <sub>50</sub> of FRET immunoassay	92
	3.5.5(e)	Verification of assay performance in human serum	93
3.5.6	FRET evaluation		95
	3.5.6(a)	Spectral overlap	95
	3.5.6(b)	FRET quenching efficiency	96
	3.5.6(c)	Förster radii	96
	3.5.6(d)	Actual donor – acceptor distance, <i>r</i>	97
3.5.7	Precision and reproducibility studies of FRET Immunoassay		98
	3.5.7(a)	Linearity and functional sensitivity	98
	3.5.7(b)	Imprecision studies	99
3.5.8	Development of Point of Care assay		101
	3.5.8(a)	Linearity and functional sensitivity	101
	3.5.8(b)	Imprecision studies	102
3.6	Conclusion		103

<b>CHAPTER 4 –</b>	<b>USE OF QUANTUM DOT IN FRET</b>	104
	<b>IMMUNOASSAY</b>	
4.1	Introduction	104
	4.1.1 Quantum dots in FRET analysis	104
4.2	Aims and objectives	106
4.3	Reagents, chemicals and instrumentations	106
4.4	Methods	107
	4.4.1 Selection of quantum dot – quantum dot FRET pair	107
	4.4.1(a) Investigation of optimal excitation wavelength	107
	4.4.1(b) Investigation of suitable quantum dots acceptor for Qd 490	107
	4.4.1(c) Determination of optimal pH	109
	4.4.2 Investigation of interaction of quantum dot with antibodies (IgG)	109
	4.4.2(a) Conjugation of quantum dot with antibodies (IgG)	109
	4.4.2(a)(i) Conjugation of IgG with quantum dot	109
	4.4.2(a)(ii) Purification	110
	4.4.2(b) Characterisation	110
	4.4.2(b)(i) SDS-polyacrylamide gel electrophoresis (SDS-PAGE)	110
	4.4.2(b)(ii) Fluorescence measurement	111
	4.4.2(c) Development of quantum dot-quantum dot FRET pair immunoassays	112
	4.4.2(c)(i) Preparation of reagents	112
	4.4.2(c)(ii) FRET immunoassay	112
	4.4.3 Investigation of interaction between quantum dot and small drug molecules	112

4.4.3(a)	Conjugation of small drug molecules to quantum dot	113
4.4.3(b)	Fluorescence measurement of the drug conjugated quantum dot	114
4.4.4	FRET studies of quantum dot as donor and organic dyes as acceptor by using monoclonal antibodies and methadone as bridge	114
4.4.4(a)	Preparation of donor molecules	116
4.4.4(b)	Preparation of acceptor molecules	116
4.4.4(c)	Interaction of antibodies conjugated Qd with organic dye label methadone molecules	117
4.5	Results and discussion	118
4.5.1	Investigation of quantum dots properties	118
4.5.1(a)	Excitation wavelength for donor molecules	118
4.5.1(b)	Selection of acceptor molecule	120
4.5.1(c)	Selection of optimum pH condition	121
4.5.2	Investigation of interaction between quantum dots and antibodies	122
4.5.2(a)	SDS-PAGE characterisation of antibodies conjugated quantum dot	123
4.5.2(b)	Fluorescence measurement of antibodies conjugated quantum dot	123
4.5.2(b)(i)	SAR conjugated Qd 490	123
4.5.2(b)(ii)	Rabbit IgG conjugated Qd 565	124
4.5.2(c)	FRET immunoassay measurement	125
4.5.2(c)(i)	Blank control assay	125
4.5.2(c)(ii)	FRET immunoassay	126
4.5.3	Investigation of interaction between quantum dots and small drug molecules	127

4.5.3(a)	Interaction of drug molecules with green quantum dots	127
4.5.3(b)	Interaction of drug molecules with red quantum dots	129
4.5.3(c)	General discussion	131
4.5.4	Interaction between quantum dot/Mab and organic dyes methadol hemisuccinate conjugate	134
4.5.4(a)	Selection of donor molecule	135
4.5.4(b)	Characterisation of the donor (Qd 525/Mab)	136
4.5.4(b)(i)	Fluorescence characterisation	136
4.5.4(b)(ii)	SDS-PAGE characterisation	136
4.5.4(c)	Study of interaction between proteins conjugated Qd 525 and LRB-EDA/Mtd	139
4.6	Conclusion	141
<b>CHAPTER 5 – EUROPIUM CHELATE AS TR-FRET DONOR FOR IMMUNOASSAY DEVELOPMENT</b>		142
5.1	Introduction	142
5.1.1	LANCE®	142
5.1.2	Cyanine 5 Amine (Cy 5)	143
5.2	Aims and objectives	144
5.3	Reagents, chemicals and instrumentations	145
5.4	Methods	145
5.4.1	Preparation of donor molecules	145
5.4.1(a)	Conjugation of Europium chelate (Eu-W1024-ITC) to anti ( <i>R</i> )-methadone monoclonal antibody (Mab)	146

5.4.1(b)	Purification of excess Europium chelate (Eu-W1024-ITC) from anti ( <i>R</i> )-methadone monoclonal antibody	147
5.4.1(c)	Characterisation of Europium chelates labelled anti ( <i>R</i> )-methadone monoclonal antibody	147
5.4.2	Preparation of acceptor (Mtd/BSA-Cy5)	147
5.4.2(a)	Conjugation of methadol hemisuccinate to bovine serum albumin (BSA)	148
5.4.2(b)	Conjugation of Cy5 amine to methadol hemisuccinate labelled BSA (Mtd/BSA-Cy5)	148
5.4.2(c)	Characterisation of acceptor (Mtd/BSA-Cy5)	148
5.4.3	TR-FRET experiment	148
5.4.4	FRET immunoassay development	150
5.4.4(a)	Optimization of donor: acceptor ratio	150
5.4.4(b)	Determination of optimum incubation time for immunoassays system	150
5.4.4(c)	Determination of IC <sub>50</sub> of TR-FRET immunoassay	150
5.4.4(d)	Verification of assay performance in human serum	151
5.4.5	Precision and reproducibility studies of TR-FRET immunoassay	151
5.5	Results and discussion	152
5.5.1	Characterisation of donor molecule (Eu/Mab)	152
5.5.2	Characterisation of acceptor molecule	152
5.5.3	TR-FRET experiment	156
5.5.4	TR-FRET immunoassay platform optimization	158
5.5.4(a)	Optimization of donor : acceptor ratio	158
5.5.4(b)	Incubation time	158

5.5.4(c)	IC <sub>50</sub> of TR-FRET immunoassay	161
5.5.5(d)	Verification of assay performance in human serum	161
5.5.5	TR-FRET evaluation	163
5.5.5(a)	Spectral overlap	163
5.5.5(b)	FRET quenching efficiency	164
5.5.5(c)	Förster radii	164
5.5.5(d)	Actual donor – acceptor distance, r	164
5.5.6	Precision and reproducibility studies of TR-FRET Immunoassay	166
5.5.6(a)	Linearity and functional sensitivity	166
5.5.6(b)	Imprecision studies	166
5.5.6(c)	Assay window and Z' factor	167
5.6	Conclusion	167
<b>CHAPTER 6 – METHOD VALIDATION OF DEVELOPED FRET BASED IMMUNOASSAYS AND ELISA WITH LIQUID CHROMATOGRAPHY – MASS SPECTROMETRY (LC-MS/MS)</b>		169
6.1	Introduction	169
6.1.1	Liquid Chromatography- Tandem Mass Spectrometry (LC-MS/MS)	170
6.2	Aims and objectives	171
6.3	Reagents, chemicals and instrumentation	171
6.4	Method	171
6.4.1	LC-MS/MS analysis	171
6.4.1(a)	Sample preparation	171

6.4.1(b)	Instrumentation	172
6.4.2	FRET based immunoassay	173
6.4.2(a)	Sample preparation	173
6.4.2(b)	Serum sample analysis & instrumentation	173
6.4.3	Point of Care FRET based immunoassay	173
6.4.3(a)	Sample preparation	173
6.4.3(b)	Serum sample analysis & instrumentation	173
6.4.4	TR-FRET based immunoassay	174
6.4.4(a)	Sample preparation	174
6.4.4(b)	Serum sample analysis & instrumentation	174
6.4.5	ELISA	174
6.4.5(a)	Sample preparation	174
6.4.5(b)	Serum sample analysis & instrumentation	174
6.5	Results and discussion	175
6.5.1	LC-MS/MS analysis	175
6.5.2	FRET based immunoassay	177
6.5.2(a)	Correlation between FRET based immunoassay with LC-MS/MS	177
6.5.2(b)	Correlation studies of FRET based Point of Care (POC) assay with LC-MS/MS	178
6.5.3	TR-FRET based immunoassay	179
6.5.3(a)	Correlation studies of TR-FRET based immunoassay with LC-MS/MS	179
6.5.4	ELISA	180
6.5.4(a)	Typical calibration curve for ELISA	180
6.5.4(b)	Correlation studies of ELISA with LC-MS/MS	181

6.5.5	Comparison of FRET and TR-FRET based immunoassay with ELISA for detection of ( <i>R</i> )-methadone	182
6.6	Conclusion	188
<b>CHAPTER 7 – CONCLUDING DISCUSSION</b>		189
7.1	General discussion	189
7.1.1	FRET based immunoassay	189
7.1.1(a)	FRET based immunoassay design	190
7.1.1(b)	Limitation factors of FRET immunoassay	191
7.1.1(b)(i)	Quantum dots	191
7.1.1(b)(ii)	Matrix effects	192
7.1.1(b)(iii)	Linearity range	192
7.1.1(b)(iv)	Assay sensitivity and accuracy	193
7.1.1(b)(v)	Hook effect	194
7.1.1(c)	Advantages of FRET immunoassay	194
7.2	Summary of the studies	196
7.3	Conclusion	197
7.4	Future perspectives	198
<b>REFERENCES</b>		199
<b>APPENDICES</b>		218



## LIST OF TABLES

		<b>Page</b>
Table 1.1	Commercially available EIA assay format.	6
Table 2.1	The weight of individual reference drug standards in the preparation of 1 mg/mL stock solution for the cross-reactivity assay.	50
Table 2.2	Checkerboard titration of anti ( <i>R</i> )-methadone monoclonal antibodies.	55
Table 2.3	Intra-assay and inter-assay of ELISA.	56
Table 2.4	Cross reactivity studies of monoclonal antibodies by direct ELISA assay.	60
Table 3.1	Donor and acceptor dye pairs.	68
Table 3.2	FRET based immunoassay parameters.	76
Table 3.3	Values of ( <i>R</i> )-methadone concentrations and FRET efficiency at different incubation time.	91
Table 3.4	Relationship between serum dilutions with FRET performance.	94
Table 3.5	Summary of FRET evaluation.	97
Table 3.6	Interday & intraday performance of FRET based immunoassay.	100
Table 3.7	Interday & intraday performance of POC assay.	103
Table 4.1	Excitation wavelengths that used for emission measurement of quantum dots.	108
Table 4.2	Solutions and concentration of SDS-PAGE.	111
Table 4.3	Amount of reagents used in conjugation process.	114
Table 4.4	Structure and molecular weight of the analyte used.	115
Table 4.5	Emission intensity of quantum dots at different excitation wavelength.	120
Table 4.6	Fluorescence quenching effect studies on drugs - Qd 525 conjugate and negative control compared to blank control.	129

Table 4.7	Studies of fluorescence intensity of drugs - Qd 650 conjugate and negative control compared to blank control.	131
Table 5.1	TR-FRET based immunoassay specification.	151
Table 5.2	Values of ( <i>R</i> )-methadone concentrations and $\Delta$ TR-FRET ratio at different incubation time.	159
Table 5.3	The matrix effect on TR-FRET ratio.	162
Table 5.4	Summary of TR-FRET evaluation.	164
Table 5.5	Interday & intraday performance of TR-FRET based immunoassay.	168
Table 6.1	Summary of electrospray ionisation parameters.	172
Table 6.2	Recovery of LC-MS/MS results on the spiked samples (n = 3).	175
Table 6.3	The estimated concentration of ( <i>R</i> )-methadone by using different analysis method.	183
Table 6.4	Comparison of analytical performance of immunoassays.	186

## LIST OF FIGURES

		<b>Page</b>
Figure 1.1	Schematics of the basic principle of heterogeneous immunoassay.	3
Figure 1.2	Schematics of the basic principle of homogeneous immunoassay.	4
Figure 1.3	Assay Principle of TRFIA. (Figure adapted from Chen <i>et al.</i> , (2015))	6
Figure 1.4	Assay Principle of FPIA. (Figure adapted from Oberleitner <i>et al.</i> ,(2015))	7
Figure 1.5	Typical configuration of lateral flow immunoassay. (Figure adapted from Branden <i>et al.</i> , (2009))	8
Figure 1.6	Jablonski diagram of FRET process. (Figure adapted from Szollosi <i>et al.</i> ,(1998))	10
Figure 1.7	Relationship between FRET efficiency with Donor-Acceptor distance. (Figure adapted from Lakowicz <i>et al.</i> , (2006a))	11
Figure 1.8	Spectral characteristic and the changes of intensity of FRET pair after FRET process. (Figure adapted from Szollosi <i>et al.</i> ,(1998))	13
Figure 1.9	(a) Molecular structures and (b) the maxima absorbance and emission of common fluorescent dyes. (Figure adapted from Medintz <i>et.al.</i> (2005) and Sapsford <i>et. al.</i> , (2006))	15
Figure 1.10	Structure of quantum dots. (Figure adapted from (Johnston, 2015))	18
Figure 1.11	Formation of exciton and its optical properties.	19
Figure 1.12	The relationship between quantum dot core materials vs its emission wavelength and its applications. (Figure adapted from Medintz, I.L., <i>et al.</i> , (2005))	20
Figure 1.13	Partial energy diagrams for the lanthanides aquo ions. (Figure adapted from Bunzli and Piguet (2005))	21
Figure 1.14	Energy pathway in sensitization of lanthanide chelate. (Bunzli and Piguet, 2005)	22

Figure 1.15	Chemical structure of aromatic amino acids in fluorescent proteins.	24
Figure 2.1	The molecular structure of methadone. (The chiral centre of the molecule is marked with *.)	29
Figure 2.2	The molecular structures of (a) ( <i>S</i> )-Methadone and (b) ( <i>R</i> )-Methadone. (The chiral centre is marked with *.)	30
Figure 2.3	Reaction scheme of synthesis of methadone. (Figure modified from (Baizer, 1953))	31
Figure 2.4	The pathway of methadone metabolism in human and major metabolites excreted in human urine. (Figure modified from Kreek <i>et. al.</i> , (1976))	37
Figure 2.5	Synthesis route of methadol hemisuccinate.	42
Figure 2.6	Synthesis of methadone-HRP.	44
Figure 2.7	Plate layout of the chequerboard study for enzyme-conjugate optimization. ( <i>R</i> )-mtd represents ( <i>R</i> )-methadone and Mab refers to monoclonal antibody.	48
Figure 2.8	ESI Mass Spectra and chemical structure of (a) ( <i>R</i> )-methadone, (b) ( <i>R</i> )-methadol and (c) ( <i>R</i> )-methadol hemisuccinate.	52
Figure 2.9	<sup>1</sup> H NMR spectrum of methadol hemisuccinate and its molecular structure with atomic numbering.	54
Figure 2.10	Average intra-assay and inter-assay calibration curve (n=6).	56
Figure 2.11	The concentration-response curve of ( <i>R</i> )-methadone monoclonal antibody against for ( <i>R</i> )-methadone.	57
Figure 2.12	Concentrations response curve of ( <i>R</i> )-methadone monoclonal antibodies towards (a) ( <i>S</i> )-methadone, (b) EDDP, (c) flunixin, (d) dextrorphan, (e) (±)-Amphetamine, (f) 11-nor-9-Carboxy- $\Delta^9$ -THC, (g) acetaminophen, (h) morphine.	59
Figure 3.1	Work flow for development of FRET based immunoassay.	67
Figure 3.2	Method for FRET immunoassay measurement.	73
Figure 3.3	Spectral overlap of fluorescence dyes suitable to pair with FITC.	78

Figure 3.4	UV-VIS spectrum of (a) native Mab and (b) FITC/Mab.	81
Figure 3.5	MALDI-TOF/TOF spectrum for (a) native Mab, (b) FITC/Mab.	82
Figure 3.6	Reaction scheme for synthesis of acceptor molecules.	83
Figure 3.7	TLC separation of acceptor molecules.	84
Figure 3.8	Mass spectrum of extracted ( <i>R,S</i> )- methadone.	85
Figure 3.9	Mass spectrum of LRB-EDA/Mtd.	86
Figure 3.10	Comparison of spectra changes between (a) positive control assay and (b) negative control assay.	86
Figure 3.11	Basic principles of FRET based immunoassay.	87
Figure 3.12	Titration of quenching efficiency on the acceptor concentration from 5 - 50 $\mu\text{g/mL}$ .	88
Figure 3.13	Emission spectra of donor molecules in different pH.	89
Figure 3.14	Measure of FRET efficiency in different pH values.	90
Figure 3.15	Relationship between incubation time and quenching percentage.	91
Figure 3.16	Plot of dose-response graph in different incubation time.	92
Figure 3.17	Typical calibration curve for mix and read FRET assay.	93
Figure 3.18	Calibration curve for FRET assays in 0.05 M borate buffer and 50 times serum dilution.	95
Figure 3.19	Excitation and emission spectra of donor and acceptor molecules. The grey shield region is the spectra overlap region.	96
Figure 3.20	Standard curve of FRET immunoassay with dynamic linear response up to 500 ng/mL.	99
Figure 3.21	Average calibration curve of (a) intraday and (b) interday (n=6).	100
Figure 3.22	Standard curve of FRET based point of care assay with dynamic linear response up to 500 ng/mL.	101
Figure 3.23	Average calibration curve of (a) intraday and (b) interday (n=6).	102

Figure 4.1	Experimental work flow.	108
Figure 4.2	Basic principle of FRET immunoassay by using quantum dot pair.	113
Figure 4.3	Basic principle of FRET immunoassay by using quantum dot – organic dye pairs.	116
Figure 4.4	Excitation (a) and emission (b) spectra of NC-490-C.	119
Figure 4.5	Emission spectra of NC-490-C (a) $\lambda_{ex}$ 400 nm and (b) $\lambda_{ex}$ 350 nm, (c) $\lambda_{ex}$ 300 nm.	119
Figure 4.6	Fluorescence emission of Qd565 at pH (a) 9, (b) 8, (c) 7, (d) 6 and (e) 5.	121
Figure 4.7	Study of fluorescence properties in different pH.	122
Figure 4.8	Emission spectra of (a) blank Qd 490 and (b) conjugate Qd 490.	123
Figure 4.9	Emission spectra of (a) un-conjugate Qd 565 and (b) conjugate Qd 565.	124
Figure 4.10	Blank FRET molecules measurements (a) blank Qd 490, (b) Qd 565/Rab and (c) mixture of blank Qd4 90 and Qd 565/Rab.	125
Figure 4.11	Emission spectra of (a) donor only control (conjugated Qd 490), (b) acceptor only control (conjugated Qd 565) and (c) mixture of donor-acceptor solution.	126
Figure 4.12	Fluorescence quenching effect studies on drugs – Qd 525 conjugate with (a) blank control, (b) salbutamol hemisuccinate, (c) lamivudine hemisuccinate, (d) stavudine hemisuccinate, (e) flunixin, (f) methadol hemisuccinate, (g) sulfonamide, (h) dextrorphan hemisuccinate.	128
Figure 4.13	Fluorescence quenching effect studies (a) blank control, (b) negative control and (c) methadol hemisuccinate Qd 525 conjugated.	128
Figure 4.14	Fluorescence quenching effect studies on drugs Qd 650 conjugate with (a) flunixin, (b) blank, (c) stavudine hemisuccinate, (d) salbutamol hemisuccinate, (e) sulfonamide, (f) lamivudine hemisuccinate, (g) methadol hemisuccinate, (h) dextrorphan hemisuccinate.	130

Figure 4.15	Fluorescence quenching effect studies (a) blank control, (b) negative control and (c) methadol hemisuccinate Qd 650 conjugated.	131
Figure 4.16	Schematic of electron exchanged process of quantum dot and drug molecules, electron hops between quantum dot and drug molecules after phonons being absorbed and release to ground state without emitting photon or through dipole-dipole energy transfer from excited quantum dot to neighbour molecule; where $h\nu'$ is the absorbed photon, LUMO is lowest unoccupied molecular orbital, HOMO is highest occupied molecular orbital and PET is photon induced electron transfer. Figure modified from Credi.A. (Credi, 2012)	134
Figure 4.17	Spectra overlapping of donors and acceptor molecules (a) emission spectra of Qd 490, (b) emission spectra of Qd 525, (c) excitation spectra of LRB-EDA/Mtd and (d) emission spectra of LRB-EDA/Mtd.	135
Figure 4.18	Emission spectra of (a) blank Qd 525 and (b) Qd 525/Mab.	136
Figure 4.19	SDS-PAGE electrophorogram with samples sequence 1 to 8 started with marker, IgG protein, Qd 490, conjugated Qd 490, Qd 525, conjugated Qd 525, Qd 565, conjugated Qd 565 for (a) fluorescence imaging under UV lamp at 365 nm, (b) UV illumination, (c) chemiluminescence illumination after destaining of Coomassie-blue.	137
Figure 4.20	Antibodies – quantum dot conjugates for left smaller size quantum dot (Qd 490/SAR), right bigger size quantum dot (Qd 565/ Rab).	138
Figure 4.21	(i) Emission spectra of (a) Mab conjugate Qd 525 and (b) mixture of conjugate QD 525 and LRB-EDA/Mtd (ii) emission spectra of (a) SAR conjugated Qd 525 and (b) mixture of blank QD 525 and LRB-EDA/Mtd. Labelled figures show the fluorescence intensity (a.u.) of the quantum dot.	140
Figure 5.1	Molecular structure of Eu – W1024-ITC	143
Figure 5.2	Molecular structure of cyanine 5 amine.	144
Figure 5.3	TR-FRET based immunoassay development.	146
Figure 5.4	Basic principles of TR-FRET based immunoassay.	149

Figure 5.5	MALDI-TOF/TOF spectrum for (a) native Mab, (b) Eu-W1024 conjugated Mab.	154
Figure 5.6	MALDI-TOF/TOF spectrum for (a) native BSA, (b) Mtd/BSA, (c) Mtd/BSA-Cy5.	155
Figure 5.7	Comparison of spectra changes between TR-FRET assay (a) and control assay (b).	157
Figure 5.8	Titration of quenching efficiency on the acceptor concentration from 1.5 – 7.5 $\mu$ M.	158
Figure 5.9	Relationship between incubation time and delta TR-FRET.	159
Figure 5.10	Plot of dose-response graph in different incubation time.	160
Figure 5.11	Typical calibration curve TR-FRET assay with 6 minutes incubation time.	161
Figure 5.12	Relationship between serum concentration and linearity range.	163
Figure 5.13	Excitation and emission spectra of donor and acceptor molecules. The grey shield region is the spectra overlap region ( $J(\lambda)$ ).	163
Figure 5.14	Presumptive FRET interaction for (a) antibody-drug system and (b) antibody-antigen system.	165
Figure 5.15	Average curve of TR-FRET immunoassay with dynamic linear response up to 1500 ng/mL.	166
Figure 5.16	Average calibration curve for (a) intraday and (b) interday (n=6).	168
Figure 6.1	MRM chromatogram of three transition characteristic for (a) blank human serum, (b) positive human serum and (c) D <sub>3</sub> -( <i>R,S</i> )-methadone in human serum.	176
Figure 6.2	( <i>R</i> )-methadone calibration curve ranging from 0 – 1000 ng/mL.	177
Figure 6.3	The comparison of serum concentration of ( <i>R</i> )-methadone between FRET based immunoassay and LC-MS/MS.	178
Figure 6.4	The comparison of serum concentration of ( <i>R</i> )-methadone between FRET based POC assay and LC-MS/MS.	179



Figure 6.5	The comparison of serum concentration of ( <i>R</i> )-methadone between TR-FRET based immunoassay and LC-MS/MS.	180
Figure 6.6	Typical calibration curve for ELISA assay.	181
Figure 6.7	The comparison of serum concentration of ( <i>R</i> )-methadone between ELISA and LC-MS/MS.	182

## LIST OF ABBREVIATIONS

%	Percent
°C	Degree Celsius
Å	Angstrom
δ	Delta, chemical shift scale
μL	Microliter
μm	Micrometer
λ	Wavelength of absorption or emission
α	Alpha
β	Beta
ns	Nanosecond
k	Kilo
Da	Dalton
3D	Three-dimensional
<sup>13</sup> C NMR	Carbon nuclear magnetic resonance
IC <sub>50</sub>	Half maximal inhibitory concentration
Δ	Delta
CHN	Carbon, hydrogen, nitrogen
TLC	Thin layer chromatography
TMS	Tetramethylsilane
d	Doublet
dd	Doublet of doublet
min	Minute
mL	Milliliter

mM	Millimolar
MS	Mass spectrometry
h	Hour
<sup>1</sup> H NMR	Proton nuclear magnetic resonance
HCl	Hydrochloric acid
LC-MS/MS	Liquid chromatography tandem with mass spectrometry
<i>J</i>	Coupling constant
K	Kelvin
FRET	Förster Resonance Energy Transfer
A	Acceptor
D	Donor
$\kappa^2$	Orientation factor
Mtd	Methadone
Mab	Monoclonal antibody
IgG	Immunoglobulin
RIA	Radioimmunoassay
EIA	Enzyme immunoassay
AP	Alkaline phosphatase
HRP	Horseradish peroxidase
TMB	K-Blue aqueous substrate
ELISA	Enzyme linked immunoabsorbent assays
EMIT	Enzyme multiplied immunoassay technique
CEDIA	Cloned enzyme donor immunoassay
FIA	Fluoroimmunoassay
FPIA	Fluorescence polarization immunoassay

LFIA	Lateral flow immunoassay
$R_0$	Förster radii
BSA	Bovine serum albumin
Mtd/BSA	Methadol hemisuccinate labelled BSA protein
CT	Charge transfer
UV	Ultraviolet
VIS	Visible range
NIR	Near infrared region
Qd	Quantum dot
Ln	Lanthanide
RE	Rare earth elements
TR-FRET	Time resolved - Förster resonance energy transfer
NADH	Nicotinamide adenine dinucleotide
FAD	Flavin adenine dinucleotide
GFP	Green fluorescent protein
YFP	Yellow fluorescent protein
trp	Tryptophan
tyr	Tyrosine
phe	Phenylalanine
MMT	Methadone maintenance treatment
pKa	Acid dissociation constant
HIV	Human immunodeficiency virus
CYP	Cytochromes P450
EDDP	2-ethylidene-1,5-dimethyl-3,3-diphenylpyrrolidine
EMDP	2-ethyl-5-methyl-3,3-diphenylpyrroline

PBS	Phosphate buffer saline
TSA	Tris-saline azide buffer
SMLs	Serum methadone levels
DMF	N,N-Dimethylformamide
DCM	Dichloromethane
EDC	N-(3-Dimethylaminopropyl)-N'-ethylcarbodiimide hydrochloride
NHS	N-Hydroxysuccinimide
$m/z$	Mass-to-charge ratio
NA	Not available
FITC	Fluorescein Isothiocyanate
LRB-EDA	Lissamine Rhodamine B Ethylenediamine
NaOH	Sodium hydroxide
ng/mL	Nanogram per milliliter
$\mu\text{g/mL}$	Microgram per milliliter
M	Molarity
nm	Nanometer
nm/s	Nanometer per second
NMR	Nuclear magnetic resonance
MALDI-TOF/TOF	Matrix-assisted laser desorption ionization tandem time-of-flight
LLE	Liquid-liquid extraction
E%	FRET efficiency in percentage
CV%	The percentage of coefficient of variance
SD	Standard deviation
$R_f$	Retention factor

LOD	Limit of detection
LOQ	Limit of quantification
SAR	Sheep anti rabbit antibody
Rab	Rabbit antibody
POC	Point of care
SDS-PAGE	Sodium dodecyl sulphate- polyacrylamide gel electrophoresis
TEMED	N, N, N', N'-Tetramethylethylenediamine
Em	Emission
Ex	Excitation
Z' factor	Indicator of assay variability
QC	Quality control

**PENYELIDIKAN MENGENAI IMUNOASAI HOMOGEN BERASASKAN  
PEMINDAHAN TENAGA RESONANS FÖRSTER UNTUK PENENTUAN  
(R)-METADON**

**ABSTRAK**

Analisis ubatan biasanya dijalankan dengan menggunakan kaedah kromatografi yang tepat dan spesifik seperti GC-MS dan LC-MS. Kaedah tersebut diketahui mempunyai kepekaan dan spesifisiti yang tinggi. Walau bagaimanapun, kaedah tersebut memerlukan peralatan yang canggih dan kepakaran profesional untuk menjalankan analisis. Bagi menganalisis sampel yang banyak, kaedah analisis yang lebih mudah seperti imunoasai akan dijalankan sebelum pengesahan keputusan dengan menggunakan GC-MS dan LC-MS. Oleh itu, asai “high throughput screening” adalah penting untuk meningkatkan kecekapan analisis perubatan. Dalam kajian ini, ciri-ciri berpendarfluor pewarna organik, titik kuantum dan kelat lantanida akan dikenal pasti kemudian digunakan. Sebagai keputusan, imunoasai homogen berasaskan FRET dan TR-FRET yang baru telah dihasilkan dan diuji untuk mengesan (*R*)-metadon dalam serum manusia. Kepekatan (*R*)-metadon dalam 50 pesakit MMT kemudian diuji. Kepekaan dan ketepatan asai yang dihasil kemudian dikaji dan disahkan dengan menggunakan kaedah LC-MS/MS. Hasil kajian juga menunjukkan bahawa terdapat kolerasi antara ketiga-tiga imunoasai dengan kaedah kromatografi. Nilai  $R^2$  daripada analisis regresi bagi imunoasai berasaskan FRET, imunoasai bersaskan “Point of Care – FRET” dan imunoasai berasaskan TR-FRET adalah  $R^2 = 0.898, 0.797$  dan  $0.910$  masing-masing. Dalam kajian ini, imunoasai yang dihasilkan akan dibandingkan dengan ELISA dari segi kepekaan, cara kendalian dan tempoh masa asai. Secara keseluruhannya, keputusan menunjukkan

bahawa imunoasai homogen yang berasaskan FRET dan TR-FRET mempunyai kelebihan berbanding dengan ELISA, kerana masa analisis yang lebih singkat dan cara pengendalian yang lebih mudah. Namun demikian, antara ketiga-tiga imunoasai, imunoasai berasaskan TR-FRET adalah kaedah analisis yang terbaik berdasarkan ketepatan dan kepekaan analisis yang tinggi. Berdasarkan keputusan ini, jelas menunjukkan bahawa imunoasai yang baru ini mempunyai potensi untuk digunakan sebagai salah satu alternatif antara asai “high throughput screening” dalam analisis perubatan. Selain itu, dapat dirumuskan bahawa titik kuantum tidak sesuai digunakan dalam kajian molekul ubat yang kecil, kerana titik kuantum didapati berinteraksi dengan molekul ubat yang kecil sama ada selepas konjugasi ataupun melalui penyerapan pasif. Oleh itu, kajian selanjutnya diperlukan untuk pemahaman antara interaksi tersebut.



**DEVELOPMENT OF FÖRSTER RESONANCE ENERGY TRANSFER  
BASED HOMOGENEOUS IMMUNOASSAY FOR DETERMINATION OF  
(*R*)-METHADONE**

**ABSTRACT**

Drug analysis is commonly performed using an accurate and specific chromatographic method, such as GC-MS and LC-MS. These methods are known to be highly sensitive and specific. However, they require sophisticated equipment and also skilled manpower for the analysis. For analysis of large number of samples, less descending methods like immunoassays are used prior to confirmation by GC-MS or LC-MS. Thus, high throughput screening is essential in increasing the efficiency of drug testing. In this study, the fluorescence properties from various types of fluorescence materials, such as organic dyes, quantum dot and lanthanide chelates were investigated and employed. As a consequence, new FRET and TR-FRET based homogeneous competitive immunoassays were successfully designed and developed for detection of (*R*)-methadone in serum sample. Then, the concentrations of (*R*)-methadone in the 50 MMT patient's serums were tested. Consequently, the accuracy and sensitivity of the developed assays were studied and validated by using LC-MS/MS method. Generally, comparison of the LC-MS/MS method with other three immunoassays methods showed adequate correlation. The regression analysis of FRET based immunoassay, point of care - FRET based immunoassay and TR-FRET based immunoassay are  $R^2 = 0.898$ ,  $0.797$  and  $0.910$ , respectively. In this study, the developed FRET based assays were also compared with conventional ELISA method in terms of assay sensitivity, simplicity of handling and assay time. Overall results suggest that the reported homogeneous immunoassays advantageous over ELISA as

it required shorter assay time with easy handling. Nevertheless, comparison among these immunoassays, TR-FRET immunoassay is the best analytical method due to its higher accuracy and sufficient sensitivity. These results demonstrated the potential of the developed immunoassays as alternatives in high throughput screening method in drug testing. Besides, through this study, it was also found that quantum dots are not suitable to be used in small drug study as there are interactions between quantum dot and small drug molecules either after conjugation or via passive adsorption. Therefore, further studies are needed to deepen the understanding of these interactions.

## CHAPTER 1

### GENERAL INTRODUCTION

#### 1.1 Drug testing

Drug abuse is an issue that brings many negative consequences to the community and also the individual (Meririnne *et al.*, 2007). In order to protect the public welfare and support the enforcement of the law, testing for drugs in urine has become important in order to defeat abuses. Most drug testing is usually carried by using highly sensitive techniques typically chromatographic and mass spectrometric techniques. However, with the recent increase in the drug abuse cases and the number of drug types (Administration, 2014), more efficient drug testing approaches, especially using high throughput screening assays have started to penetrate into drug testing laboratories.

The drug testing process starts by using low cost screening analysis as initial tests and suspect samples are further confirmed using a more accurate method such as chromatographic analysis and mass spectrometry (Kankaanpää *et al.*, 2004). The common screening methods that are used in drug testing laboratories are thin-layer chromatography (TLC) and immunoassays.

Thin-layer chromatography is a primary screening test that is low in cost and able to be rapidly performed by spotting the sample on a TLC plate (Kenyon *et al.*, 1995). The results are reliable as identical drugs or analytes will always give same migration pattern ( $R_f$  value). Besides, it is also able to separate the target drug and its metabolite as spots on the plate. However, this method lacks of sensitivity and specificity. The accuracy of the result decreases when the concentration level of the

analyte is low. In addition, it only allows qualitative determination and frequently results in false positives (Schütz *et al.*, 2006).

On the other hand, immunoassays allow or both qualitative and quantitative analysis and is relatively sensitive (Hoofnagle and Wener, 2009). It does not use sophisticated equipment and immunoassays provides a flexible and rapid way to screen large number of samples in a short period of time (Darwish, 2006). As immunoassays are one of the most cost effective ways for drug detection, it has become a preferred screening technique (Gan and Patel, 2013).

## **1.2 Immunoassay**

Immunoassay is a diverse technique that utilizes the interaction of the antigen (target substances) with antibodies. The first immunoassay was published by Dr. Solomon Berson and Dr. Rosalyn Yalow for the analysis of insulin (Yalow and Berson, 1960). The radioimmunoassay (RIA) for insulin was clinically significant and Dr. Rosalyn became the co-winner for the Nobel Prize in Medicine/Physiology in 1977 (Wu, 2006).

Immunoassay is the measurement of the degree of binding between an antibody and a target analyte. To perform this measurement, labels such as radioactive isotopes, fluorescent tags or enzymes are usually used. The change in the reading of the label when bound to the antigen is the basis of measurement for the instrument. Generally, it can be performed in either heterogeneous or homogenous phase (Jiang *et al.*, 2011).

In a heterogeneous system, either antibodies or antigens will be immobilized onto a solid phase, and the analytes or the detection molecules (typically in aqueous phase) are added sequentially. In order to remove the free analytes from antibody bound analytes, separation or washing steps are performed. The signal from the system is then obtained from the measurement of the labelled antigen that is bound on the solid surface (Figure 1.1).

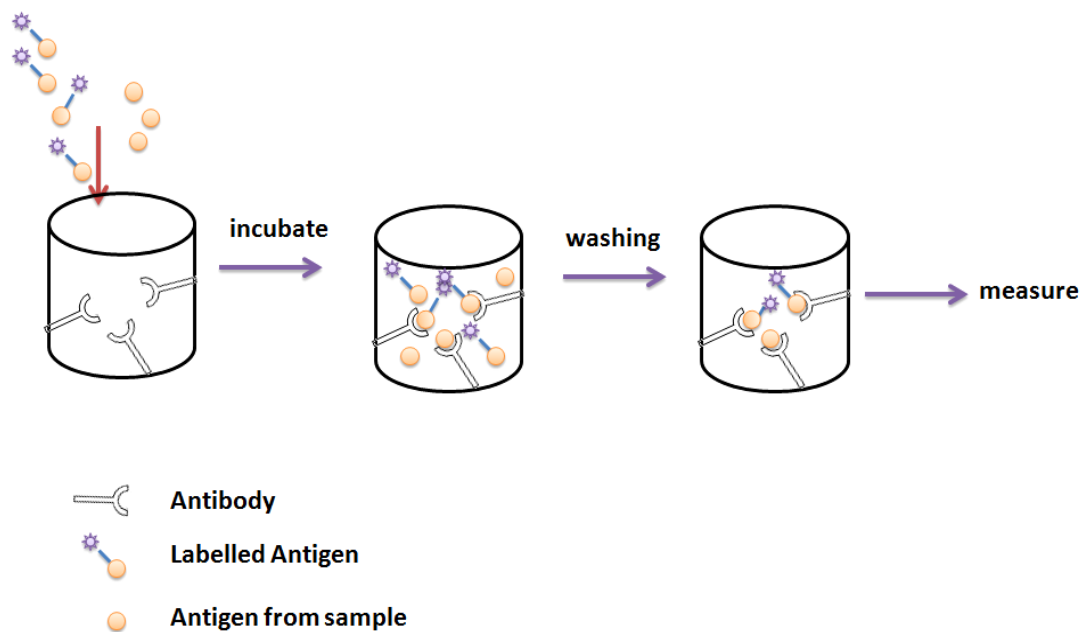


Figure 1.1: Schematics of the basic principle of heterogeneous immunoassay.

In contrast to the heterogeneous system, homogeneous phase analysis generally involves the conjugation of the biomolecules to the labelling materials that is used for signal enhancement. The formation of immunocomplex is performed in a solution phase by adding the analyte and labelled analyte with the antibodies. The binding of the labelled analyte with the antibody will then alter the signal of the labelled analyte and hence reports the outcome (Figure 1.2) (Dasgupta and Wahed, 2014).

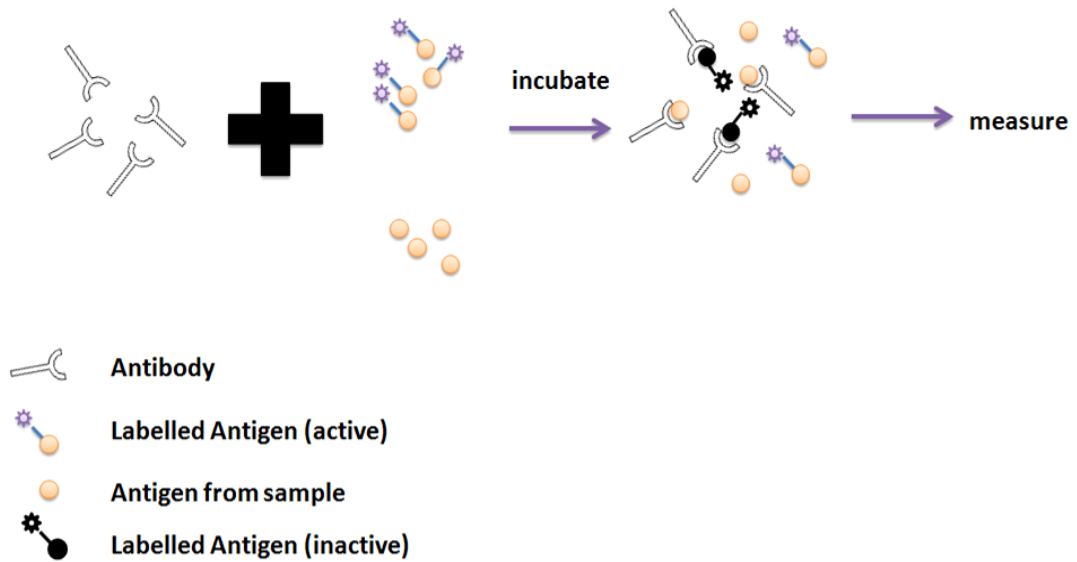


Figure 1.2: Schematics of the basic principle of homogeneous immunoassay.

### 1.2.1 Immunoassay system in drug testing

To date, scientists have utilized the unique features of immunoreactions (capable of drug detection in complex samples) in development of immunoassay for use in drug testing. There are 4 main types of detection methods that are commonly used in drug screening.

#### 1.2.1(a) Radioimmunoassay (RIA)

Radioimmunoassay is a heterogeneous assay system that is based on the measurement of the quantity of radioactive isotopes that are bound to the antibodies. In the assay, the free antigen will compete with the isotope-labelled antigen to bind to the antibody. After the reaction, the unbound analyte and analyte-indicator will be removed from the system through a washing or separation step. RIA commonly utilizes iodine-125 as the indicator for signal enhancement. This isotope exhibits a relatively short life time of 60 days and frequent resynthesizing of the reagent is required (Weeks *et al.*, 2013).

However, the issue of radioactive waste disposal has led to the recent drop in popularity of RIA usage. Besides that, the specialized and high cost equipment is needed for the measurement. Thus, RIA is gradually being replaced by other easily automated immunoassay systems in spite of it being able to produce accurate results (Goldsmith, 1975).

### **1.2.1(b) Enzyme immunoassay (EIA)**

Enzyme immunoassay is the further improvement for the RIA system as it is based on the same reaction principles. Generally, the desired target drug analytes are labelled to enzymes instead of radioactive isotopes in the assay system. The signal is later detected by the after competitive reaction between the drug labelled enzyme and free drug molecules. To date, there are both heterogeneous and homogeneous EIA assay formats available in the market (Lequin, 2005).

Many enzyme based immunoassay systems have been developed and commercialized for drug screening purpose, such as Enzyme-Linked Immunosorbent Assay (ELISA), Enzyme Multiplied Immunoassay Technique (EMIT) and Cloned Enzyme Donor Immunoassay (CEDIA) (O'Kennedy *et al.*, 1990; Porstmann and Kiessig, 1992). These assays were designed by using different labels for signal enhancement and the format of these assays is summarized in Table 1.1. However, pros and cons of the different platforms have to be considered when choosing the right platform for the desired sensitivity and specificity of analysis.

Table 1.1: Commercially available EIA assay format.

Immunoassay	Format	Enzyme
ELISA	Heterogeneous	Alkaline phosphatase (AP) & Horseradish peroxidase (HRP)
EMIT	Homogeneous	glucose 6-phosphate dehydrogenase enzyme
CEDIA	Homogeneous	beta-galactosidase

### 1.2.1(c) Fluoroimmunoassay (FIA) & Fluorescence polarization immunoassay (FPIA)

Just like other immunoassays, fluoroimmunoassay also relies on the interaction of fluorescent material (typically lanthanide chelates complexes) labelled proteins with the target molecules. It can be performed in both homogeneous and heterogeneous phase which typically involve the usage of secondary antibody. The fluorescence properties which are altered by the interaction between the antibodies and antigens will report the outcome. Due to the high sensitivity of the assay, the applications of fluoroimmunoassays are tremendous and it is readily available in the market as dissociation enhanced lanthanide fluoroimmunoassays (DELFLIA) or time-resolved fluoroimmunoassays (TRFIA) (Hemmila, 1985; Vohr, 2005).

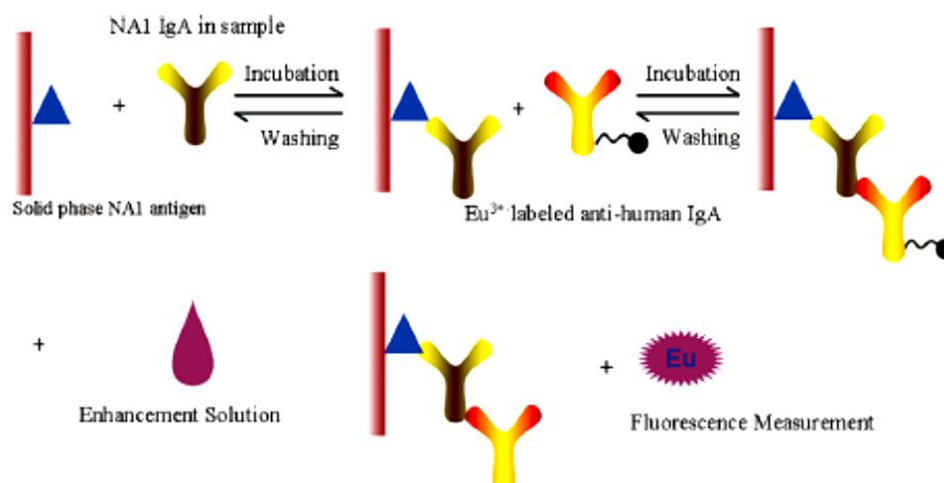


Figure 1.3: Assay Principle of TRFIA. (Figure adapted from Chen *et. al.*, (2015))



There is another type of fluorescent labelled based immunoassay in the market which is called fluorescence polarization immunoassay (FPIA). FPIA is performed in homogeneous phase and the detection signal of FPIA is obtained through the behaviour of the fluorophore labelled antigen under the plane-polarized light (Figure 1.4). The interactions of the free drug molecule in the samples, fluorophore labelled reagents and antibodies can be correlated to the drug levels in the samples through a calibration curve (Routledge and Hutchings, 2013).

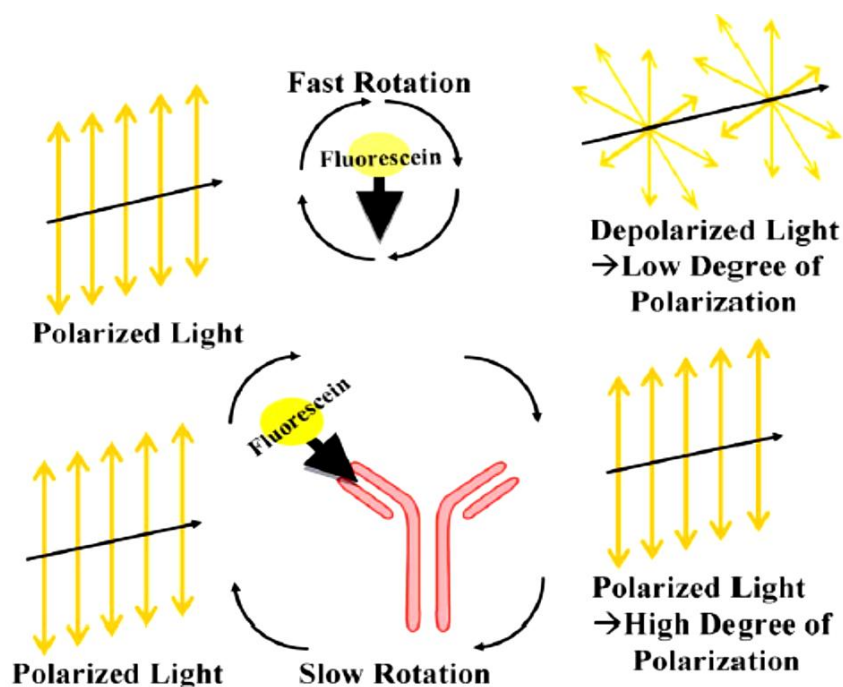


Figure 1.4: Assay Principle of FPIA. (Figure adapted from Oberleitner *et al.*(2015))

#### 1.2.1(d) Lateral flow immunoassay (LFIA)

Lateral flow immunoassay, also called immunochromatographic tests, is a specially designed point of care (POC) testing device. A recent published review had emphasized its sensitivity, selectivity and ease of use of this assay method (Sajid *et al.*, 2015; Posthuma-Trumpie *et al.*, 2009). LFIA consists of several assay formats where the formats are chosen depending on the analyte. The labelling materials that are often used in FLIA are nanoparticles such as colloidal gold, iron oxide magnetic

particles, fluorescent and luminescent materials, colloidal carbon and enzyme. These labelling materials normally exhibit high stability and also able to detect at low concentration (Sajid *et al.*, 2015).

In LFIA, there is a surface layer (sample pad) to collect the sample and a layer of conjugate pad that consists of desired labelled biomolecules. The added sample will travel through the conjugate pad and interact with the labelled biomolecules in it. Together, the sample and labelled molecules will then continue to flow along the strip (detection zone) up to the absorbent pad. This will allow chromatographic separation of the excess target drugs and hence increase the sensitivity of the assay. The typical configuration of lateral flow immunoassay is shown in Figure 1.5.

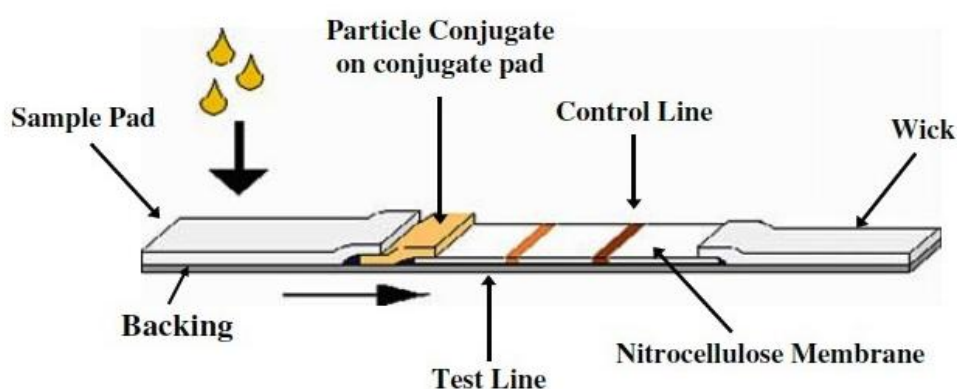


Figure 1.5: Typical configuration of lateral flow immunoassay. (Figure adapted from O'Farrell *et al.*, (2009))

### 1.2.2 Heterogeneous vs homogeneous immunoassay

As mentioned previously, a separation step (or a washing step) prior to signal measurement is required in heterogeneous assays. Consequently, the matrices or interferences are able to be removed and hence increasing the sensitivity of the assay.

However, homogeneous immunoassays are more user friendly and have faster assay time as it does not require the separation step (Schütz *et al.*, 2006; Wild, 2013). Besides that, it also allows the analysis of complex samples, such as unprocessed blood and urine samples (Pei *et al.*, 2013). These unique features have fascinated researchers in utilizing homogeneous immunoassay in drug testing. As such, Förster Resonance Energy Transfer technique that is based on fluorescent labelled offers a good prospect in development of brand new homogeneous immunoassay.

### **1.3 Förster Resonance Energy Transfer (FRET)**

Förster resonance energy transfer (FRET) is a theory of molecular resonance energy transfer that was published by Theodor Förster in 1946 (Theodor, 1946). This theory described the non-radiative interaction of an electronic excited molecule with the near-neighbour molecule within distance of 10 – 100 Å (Theodor, 1948; Clegg, 1995).

When there is a matching energy frequency at the vibration level between two molecules, it can be said that there is a resonance condition between these two molecules. Hence, the energy which has the same frequency between these two near-neighbour molecules is able to transfer non-radiatively from one to another upon excitation. This energy transmission typically occurs from the donor molecules to the acceptor molecules (Schmid and Sitte, 2003). The Jablonski diagram of the energy transfer pathway is shown in Figure 1.6.

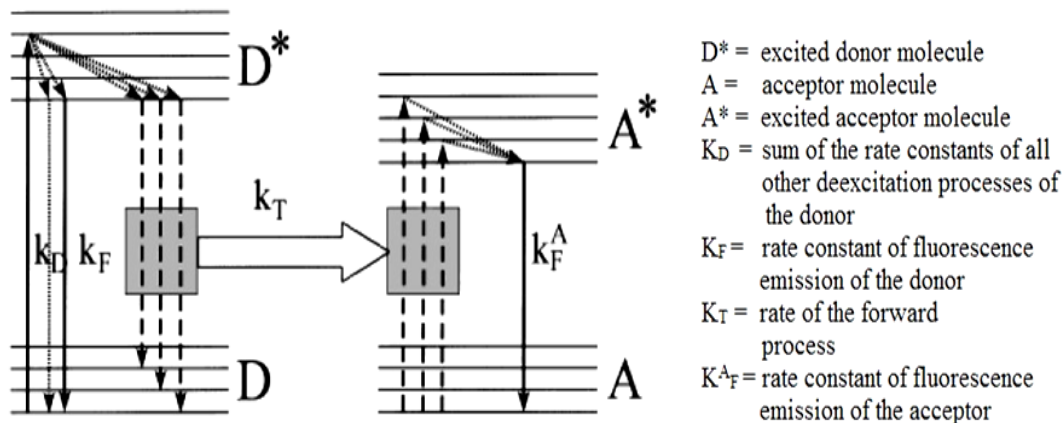


Figure 1.6: Jablonski diagram of FRET process. (Figure adapted from Szollosi *et al.*,(1998))

This energy transmission is the result of long range dipole-dipole interactions between the donor and acceptor molecules. This resonance energy transfer can clearly be observed when it occurs between a fluorophore and an acceptor molecule. As a result of this energy transfer, the donor molecule’s fluorescence intensity and excited lifetime is reduced. Subsequently, the acceptor molecule will be sensitized and its fluorescence intensity will increase (Figure 1.8). This pair of interacting fluorescent molecules is referred to as donor/acceptor pair or FRET dye pair (Masters, 2014).

### 1.3.1 FRET Efficiency

The signal measurement for FRET analysis is done by calculating the amount of quanta (energy) being transferred from donor to acceptor, which is called FRET efficiency (Clegg, 1995). FRET efficiency can be calculated either by measuring the change in lifetime or the intensities changes of the donor fluorophore as defined in Equation 1.1 below:

$$E = 1 - \frac{\tau_{DA}}{\tau_D} = 1 - \frac{F_{DA}}{F_D} \quad [1.1]$$

where  $E$  is the quantum yield of energy transferred,  $\tau_{DA}$  is the lifetime of the donor with the acceptor and  $\tau_D$  is the lifetime of the donor without the acceptor;  $F_{DA}$  is the emission intensity of the donor with the acceptor and  $F_D$  is the emission intensity of the donor without the acceptor (Lakowicz, 2006a).

### 1.3.2 Factors that affect FRET efficiency

There are a few factors that need to be considered and satisfied to facilitate FRET.

#### 1.3.2(a) Distance between donor-acceptor molecules

FRET strongly depends on the distance between the donor and acceptor molecules. It only happens when the two interacting molecules are sufficiently close, typically within 10 – 100 Å (Hayward *et al.*, 2010). Förster defined the relationship between the distance between the two interacting molecules with the FRET efficiency in the equation below.

$$E = \frac{R_0^6}{R_0^6 + r^6} \quad [1.2]$$

where  $R_0$  is the Förster radius where 50% of energy is transferred; while  $r$  is the distance between donor and acceptor molecule (Figure 1.7).

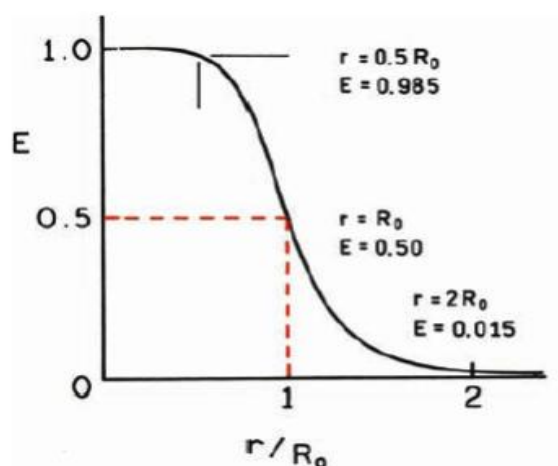


Figure 1.7: Relationship between FRET efficiency with donor-acceptor distance. (Figure adapted from Lakowicz (2006a))

$R_o$  may also be affected by other parameters and their relationship as shown in the equation below.

$$R_o^6 = \frac{9000(\ln 10)\kappa^2 Q_D}{128\pi^5 N n^4} \int_0^\infty F_D(\lambda) \varepsilon_A(\lambda) \lambda^4 d\lambda \quad [1.3]$$

where  $\kappa^2$  is the orientation factor,  $Q_D$  is the quantum yield of the donor,  $N$  is the Avogadro's number,  $n$  is the refractive index of the medium,  $F_D(\lambda)$  is the corrected fluorescence intensity of donor from  $\lambda$  to  $\lambda+\Delta\lambda$  with the total intensity normalized to unity.  $\varepsilon_A(\lambda)$  is the extinction coefficient of the acceptor at  $\lambda$  nm in unit  $M^{-1}cm^{-1}$  (Lakowicz, 2006a).

### 1.3.2(b) Spectral overlap of donor and acceptor

The matching of emission and excitation spectra (spectral overlap) between donor molecule and acceptor molecule is necessary in order for FRET to occur. Generally, the donor molecule emits at a shorter wavelength, and this emission wavelength needs to overlap with the excitation wavelength of the acceptor molecule. The degree of spectral overlapping may affect the efficiency of energy transmission. The FRET process occurs significantly when the achieved overlap is more than 30 (Stryer, 1978). The degree of spectral overlap which is also referred as spectral overlap integral ( $J$ ) can be calculated through the following equation.

$$J(\lambda) = \int_0^\infty F_D(\lambda) \varepsilon_A(\lambda) \lambda^4 d\lambda \quad [1.4]$$

where  $F_D(\lambda)$  is the corrected fluorescence intensity of the donor from  $\lambda$  to  $\lambda+\Delta\lambda$  with the total intensity normalized to unity,  $\varepsilon_A(\lambda)$  is the extinction coefficient of the

acceptor at  $\lambda$  nm in unit  $M^{-1}cm^{-1}$ (Lakowicz, 2006a). The spectral characteristic and the changes of the intensity of the FRET pair after FRET process is summarized in Figure 1.8 below.

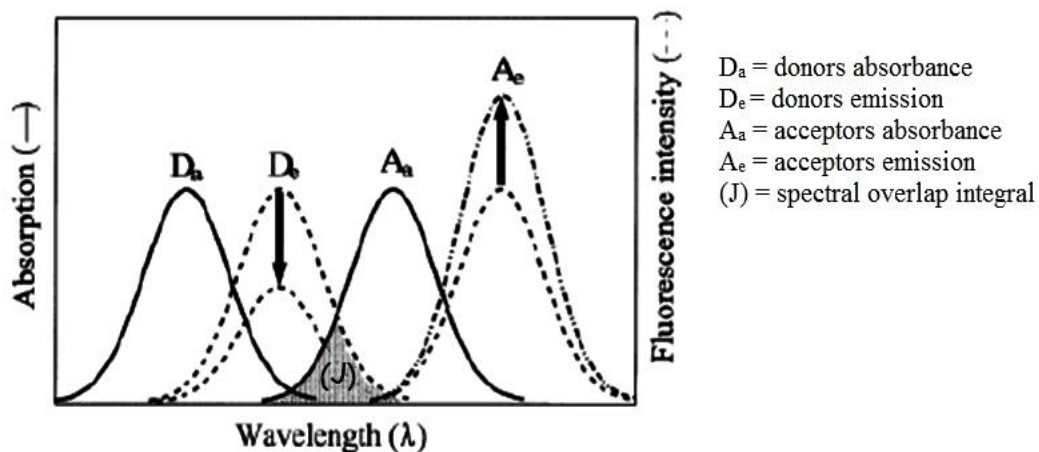


Figure 1.8: Spectral characteristic and the changes of intensity of FRET pair after FRET process. (Figure adapted from Szollosi *et al.*, (1998))

### 1.3.2(c) Transition dipole orientations of the donor and acceptor

The transition dipole orientation of the donor and the acceptor in the FRET system is expressed as the orientation factor,  $\kappa^2$ . It is one of the important parameters in the calculation of Förster radii (Khrenova *et al.*, 2015). In order to FRET, the transition dipole of the donor molecules and the acceptor molecules have to be approximately parallel. The transition conformation of the donor and acceptor molecules can vary from range  $0 \leq \kappa^2 \leq 4$  (Loura, 2012).

Generally,  $\kappa^2$  is always assumed equal to be  $2/3$  because this is the value for the transition orientation of donor or acceptor species where it is randomized by rotational diffusion before energy transfer. In fact, the orientations of donor and acceptor species (macromolecules in this case) are likely to be randomized when tagged with fluorophores. In addition to that, research have also proved that the

errors when calculating the distance is less than 35% when assuming  $\kappa^2 = 2/3$ . This finding further strengthens this assumption (Lakowicz, 2006a).

### **1.3.3 Fluorescent materials for used in FRET system**

One of the important criteria of FRET is that it explains the pathway of the excited photon in the donor molecule returning to its ground state through the transfer of its excitation energy to another proximate molecule (Chirio-Lebrun and Prats, 1998). This process generally involves at least one fluorescent material as the donor molecule and an acceptor molecule that must be able to absorb the energy from donor at the donor's emission wavelength. Although the acceptor molecule does not necessarily have to be fluorescent, most users however are likely to use fluorophore as donor and acceptor in their FRET system (Cardullo, 2007). In general, there are several fluorescent materials that are being utilized in FRET system. The details are described below:

#### **1.3.3(a) Organic dyes**

Organic dyes also referred to as fluorescent dyes or fluorophores, are small organic molecules of 20 - 100 atoms that contain polyaromatic hydrocarbons or heterocycles in their molecular structure. The optical properties of organics dyes come from the nature of the electron transition over the fluorophore. Briefly, emission happen when there is formation of charge transfer (CT) state (CT dyes), transmission of delocalized electron between energy band or electronic state (mesomeric dyes) over the fluorophore (Resch-Genger *et al.*, 2010).



Organic dyes are categorised under the group of extrinsic fluorescent materials. It is able to absorb and emit light readily in the longer wavelength, which could be in ultraviolet (UV), visible range (VIS) and near-infrared (NIR) region. The common structures of commercially available fluorescent dyes that absorb and emit at different wavelengths along with the spectral region is shown in Figure 1.9 (Sauer *et al.*, 2011).

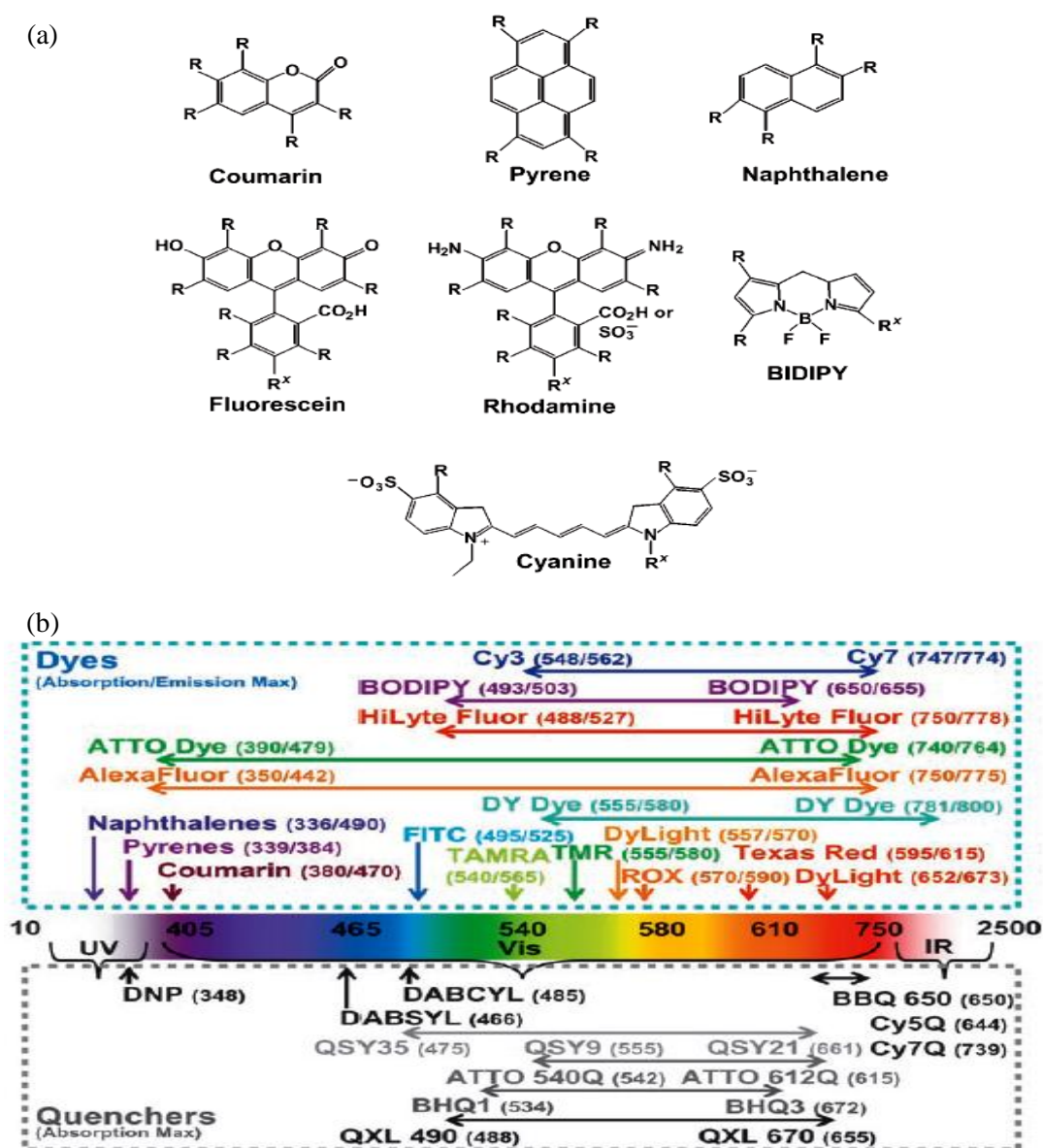


Figure 1.9: (a) Molecular structures and (b) the maxima absorbance and emission of common fluorescent dyes. (Figure adapted from Medintz *et al.* (2005) and Sapsford *et al.*, (2006))

Fluorophores are one of the powerful tools in biological research. They are popular as they have a high extinction coefficient ( $10,000 - 100,000 \text{ M}^{-1}\text{cm}^{-1}$ ) and a high quantum yield (Lakowicz, 2006d). Consequently, organic dyes are excellent in absorbing light and able emit fluorescence efficiently. Also, their fluorescence life time ranges between 1 – 10 ns and they decay at a mono-exponential rate (Resch-Genger *et al.*, 2008; Lakowicz, 2006d).

Each fluorescent dye has its own unique fluorescence properties where their fluorescence intensity and also wavelength can be altered readily by solvent polarity, pH, temperature and also voltage of the environment (Sauer *et al.*, 2011; Sousa *et al.*, 1996). Generally, organic dyes are very soluble and stable in water. There are, however, some fluorescent dyes like cyanine dyes and certain fluorescein derivatives that have low solubility in water. Furthermore, reactive functional groups can often be found in fluorescent dyes (Sapsford *et al.*, 2006). This enables the conjugation of fluorophores to biomolecules to be easily carried out and further extend their applications, especially in FRET assays.

Unfortunately, most fluorescent dyes have low photochemical stability. They decompose easily and experience fading of fluorescence intensity when exposed continuously to light or upon repeated excitation. This phenomenon is also called photobleaching. Besides, the broad absorption/emission profile and small stoke shift may lead to high background reading and spectral bleed through. This spectral bleed through will lead to the detection of fluorescence from an undesired fluorophore (typically from the second fluorophore) and will definitely complicate the FRET analysis (Feng *et al.*, 2006; Sapsford *et al.*, 2006).

Despite these drawbacks, fluorophores are indispensable in applications in biology. The use of organic dyes is cost effective and the ease of bioconjugation reduces the burden on the investigators. Furthermore, new approaches on producing novel organic dyes with better chemical and optical properties may also further extend the use of organic dyes in FRET analysis (Bai *et al.*, 2007; Zhao *et al.*, 2013).

### **1.3.3(b) Inorganic materials**

Inorganic fluorescent materials are usually associated with the doping of relatively inert matrices such as zinc sulphide or cadmium sulphide with activator metallic ions such as transition or rare earth elements (Williams, 1980). Inorganic fluorescent materials have broad Stokes shift and they usually need to be excited at ultraviolet or near visible region. Besides that, they also display longer fluorescence lifetime when compared to organic dyes. These unique features have enhanced the usage of inorganic fluorescent materials in FRET analysis (Lakowicz, 2006d). They are generally mildly toxic. Among all inorganic fluorescent materials, quantum dots and lanthanide complexes are frequently used by researchers in FRET studies. The details are described as below.

#### **1.3.3(b)(i) Quantum dots**

Quantum dots are semiconductor nanocrystals that are composed of an inorganic core and an outer layer which is normally capped with a layer of surfactant molecules (ligands) or metal shell in order to avoid agglomeration (Reiss, 2008). Generally, the quantum dots' inorganic core can be made from semiconductor metals, alloys and other metals such as gold. The inorganic core normally contain a tiny droplet of free electrons (Ghasemi *et al.*, 2009) and they are in spherical shape with diameters ranging from 1 to 10 nm.

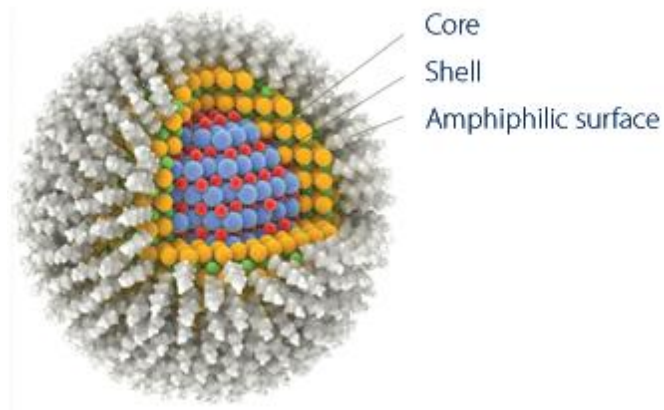


Figure 1.10: Structure of quantum dots. (Figure adapted from (Johnston, 2015))

These relatively small particle size enable quantum dots to display special electronic properties which is referred as quantum confinement effect (Frasco and Chaniotakis, 2009). As the particle sizes reduced down to a few nanometers, the wavelength of the electron (Bohr radius) becomes bigger than the nanocrystals. Hence, the confining dimension of the electrons decreases and these electrons then respond to the changes in its energy levels. Subsequently, the formation of energy level structure changes from band-like levels (typical bulk semiconductor energetic structure) into discrete-like levels (discrete molecules energy level).

These unusual situations cause the formation of larger spacing between the energy bands (conduction and valence band) and ultimately the band gap energy level will increase. As such, the movement of electrons between two energy levels lead to the formation of exciton (Figure 1.11), which is also referred to as electron-hole pairs (Reiss, 2008; Feng *et al.*, 2006).

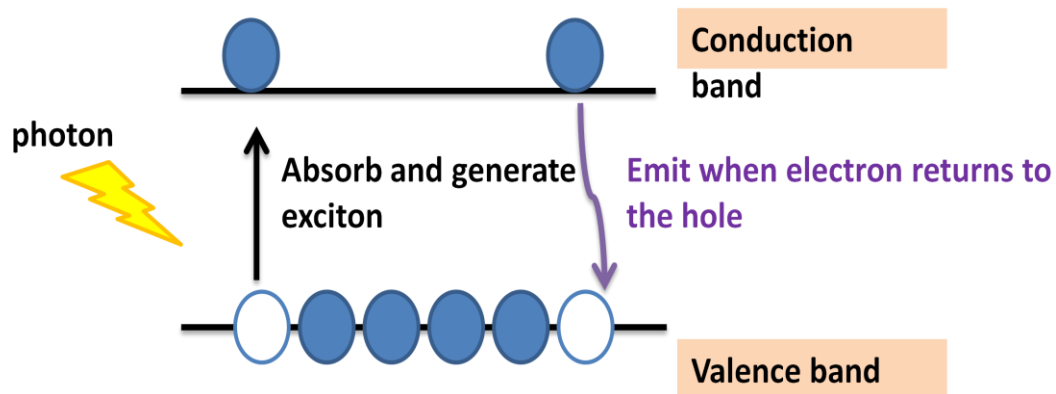


Figure 1.11: Formation of exciton and its optical properties.

The optical properties of quantum dots are the result of the movement of electrons between the valence band and the conduction band (Figure 1.11). The 3D quantum confinement of the electrons and holes (exciton) enhances their optical properties through the controlling of the size of the crystal structure. Also, quantum dots show large stoke shift by displaying continuous absorption spectra from ultraviolet to visible region and show narrow size-tunable emission spectra width (Valeur and Berberan-Santos, 2012; Reiss *et al.*, 2009; Resch-Genger *et al.*, 2008).

Different elements and composition may lead to different chemical and physical properties of quantum dots (Figure 1.12). Besides that, the inorganic shell that is coated at the outer layer of the core of the quantum dots have further enhanced the stability of the quantum dots towards photodegradation (Rizvi *et al.*, 2010; Baranov *et al.*, 2003) and provide higher photochemical stability in comparison to organic dyes (Resch-Genger *et al.*, 2008). Quantum dots exhibits longer fluorescence life times which is in range of 10 – 100 ns and typically experience a multi-exponential decay rate.

All these characteristics are able to broaden the usage of quantum dots in many applications, such as optical coding, biosensor and imaging, photoelectrochemistry application and also as FRET donor (Figure 1.12).

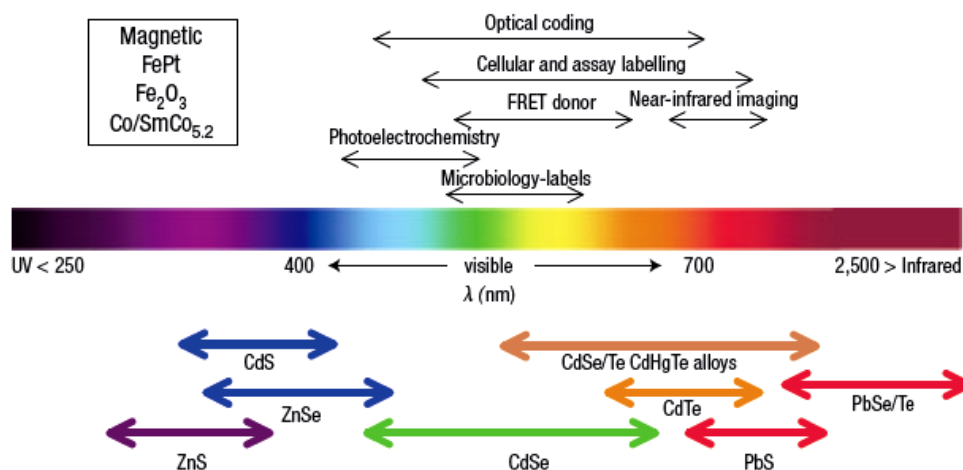


Figure 1.12: The relationship between quantum dot core materials vs its emission wavelength and its applications. (Figure adapted from Medintz, *et al.*, (2005))

### 1.3.3(b)(ii) Lanthanides

Lanthanide elements (Ln) also referred as rare earth elements (RE), are elements with atomic numbers ranging from 57 to 71 (from lanthanum to lutetium). They are also known as f-block elements with the general electronic configurations of  $[Xe]4f^{n-1}5d^16f^2$ . They exhibit metal-like properties and a stable +3 oxidation state (Huang and Bian, 2010).

The trivalent lanthanide ions have unfilled 4f shells, and thus different energy levels are generated through different arrangements of electrons in the 4f shell. Consequently, numerous absorption and emission spectra ranging from UV to visible and near-infrared (NIR) can be generated through the electron transition between the various energy levels (Figure 1.13). These 4f electron transitions make most

lanthanides ions luminescent and exhibit line like emission spectra (Bunzli and Piguet, 2005; Huang and Bian, 2010; Binnemans, 2009; Hemmila and Laitala, 2005).

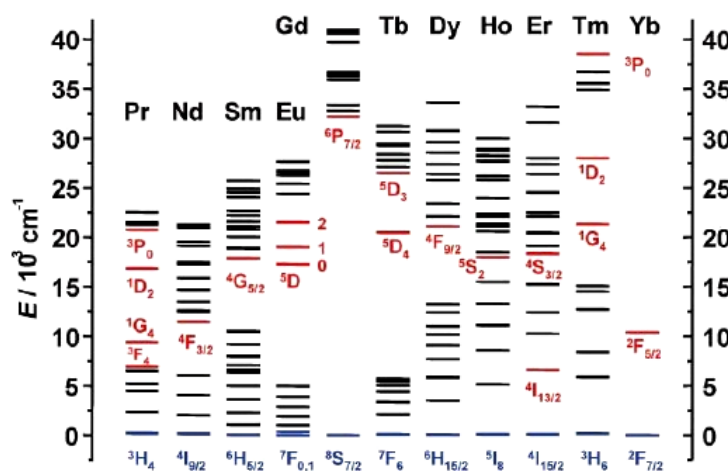


Figure 1.13: Partial energy diagrams for the lanthanides aquo ions. (Figure adapted from Bunzli and Piguet (2005))

However, the usage of lanthanide ions is limited due to their low molar absorption coefficients (typically less than  $10 \text{ M}^{-1}\text{cm}^{-1}$ ). Hence, lanthanide ions are often coupled with intense absorption organic chromophores in order to stimulate the antenna effect. Here, the organic chromophore will absorb the excitation energy, and then transfer this energy to the lanthanide ion by intramolecular energy transfer. The lanthanide ions will then be sensitized and emit light at a well defined wavelength (Binnemans, 2009; Bunzli and Piguet, 2005; Chen and Xu, 2010; Matsumoto *et al.*, 2002; Hemmila and Laitala, 2005) (Figure 1.14). This phenomenon also causes lanthanide chelates to exist longer fluorescence lifetimes ( $10^{-2} - 10^{-6} \text{ s}$ ) as compared to conventional fluorophores ( $10^{-8} - 10^{-10} \text{ s}$ ) (Huang and Bian, 2010).

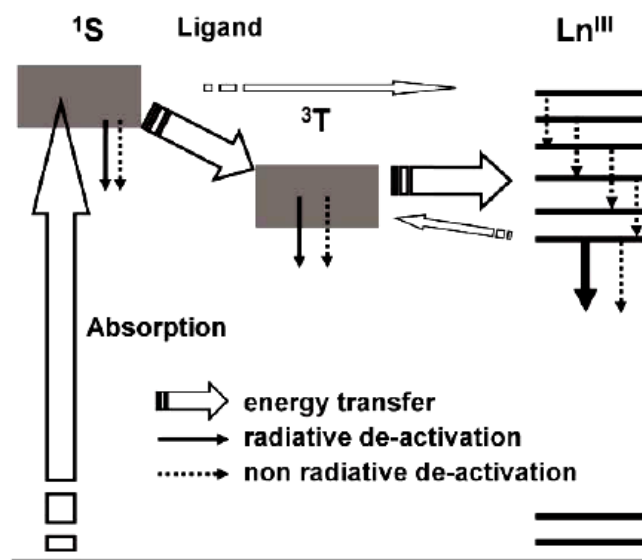


Figure 1.14: Energy pathway in sensitization of lanthanide chelate. (Bunzli and Piguet, 2005)

These unique luminescent features of lanthanide chelates have fascinated researchers and help expand its applications such as electronic display to biological assays in biomedical applications (Selvin, 2002; Werts, 2005). Among all the lanthanide chelates, europium and terbium have highest emission intensity in the visible region. Thus, they have gained a lot of popularity in bioanalytical applications especially in the development of time resolved – FRET (TR – FRET) based assay (Sapsford *et al.*, 2006).

Scientists have reported that there are a few advantages when utilizing lanthanide chelates as donor in FRET system. Firstly, the line-like emission spectra and long decay time of lanthanide chelate reduces the background fluorescence effects. Furthermore, the long decay time also enhances efficient dynamic energy transfer and diminishes the orientational factor effect ( $\kappa^2$  value) in FRET system (Hemmila and Laitala, 2005).



Also, the environment polarity-independent spectral properties that make the luminescence intensity and peak free from solvent polarity can also further enhance the usage of lanthanide in development of TR-FRET based assay (Lakowicz, 2006d). In addition, the broad peak like emission spectra of lanthanide chelates had increases the possibility of spectral overlapping and allow a wide range of acceptor dyes to couple with it (Sapsford *et al.*, 2006). Consequently, assay sensitivity can be increased.

In view of this, a lot of efforts have been made by researchers to utilized lanthanide chelates in TR-FRET studies. A large number of conjugatable chelators that are able to displace the bound water molecules have been synthesised and described (Lakowicz, 2006d). However, there are still some uncertainties when using the currently available chelators (Sapsford *et al.*, 2006). Thus, careful investigation is still needed when using lanthanide chelates in TR-FRET studies.

### **1.3.3(c) Fluorophore of biological origin**

Unlike organic or inorganic fluorophores, fluorophores of biological origin are intrinsic fluorophores with natural fluorescence. Usually, they are enzymatic cofactors such as nicotinamide adenine dinucleotide (NADH) and flavin adenine dinucleotide (FAD) or fluorescent proteins such as green and yellow fluorescent proteins (GFP, YFP). The usage of these intrinsic fluorescent compounds in FRET analysis were always emphasized (Sapsford *et al.*, 2006).

Fluorescent proteins contain aromatic amino acid residues such as tryptophan (trp), tyrosine (tyr) and phenylalanine (phe) (Figure 1.15) and these enhance their fluorescence properties (Lakowicz, 2006b). These biological fluorescent compounds features strong absorbance at UV region and emission at VIS region with a fluorescence lifetime of not more than 7 ns. Compared to organic or inorganic fluorophores, fluorescent proteins are known to have lower quantum yield (<0.01 – 0.35) and poor photo stability (Sauer *et al.*, 2011). These features somehow limit the usage of fluorescent proteins in biological applications.

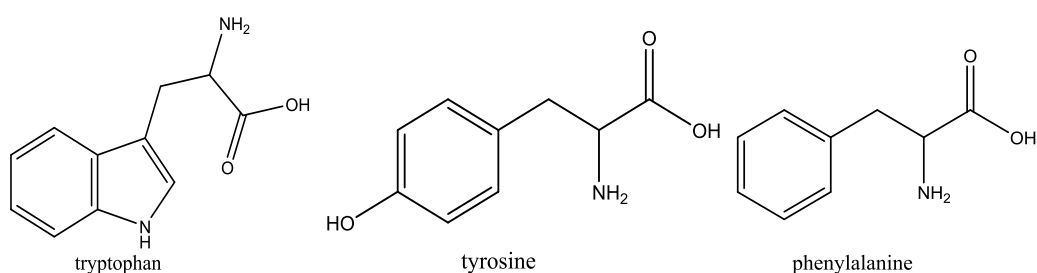


Figure 1.15: Chemical structure of aromatic amino acids in fluorescent proteins.

Several disadvantages are observed when using fluorescent protein in FRET analysis. The big protein size (25 – 30 kDa or larger) and the broad absorbance and emission spectra will lead to the cross talk effect (also terms as spectral bleed through) and ultimately decrease the FRET efficiency. In addition, the restricted excitation region of the fluorescent proteins confine the FRET donor-acceptor to be paired only in the UV region (Sapsford *et al.*, 2006). Furthermore, the interaction between these fluorescent proteins with other fluorescent proteins may lead to self-quenching in the fluorescence intensity during FRET analysis (Piston and Kremers, 2007).